AFRL-RY-WP-TP-2011-1007

AN ALTERNATIVE TREATMENT OF HEAT FLOW FOR CHARGE TRANSPORT IN SEMICONDUCTOR DEVICES (POSTPRINT)

Matt Grupen

Electro-optic Components Technology Branch
Aerospace Components Division

JULY 2010

AIR FORCE RESEARCH LABORATORY
SENSORS DIRECTORATE
WRIGHT-PATTERSON AIR FORCE BASE, OH 45433-7320
AIR FORCE MATERIEL COMMAND
UNITED STATES AIR FORCE

REPORT DOCUMENTATION PAGE

Form Approved
OMB No. 0704-0188

1. REPORT DATE *(DD-MM-YY)*	2. REPORT TYPE	3. DATES COVERED *(From - To)*
July 2010	Journal Article Postprint	15 September 2008 – 31 July 2010

4. TITLE AND SUBTITLE
AN ALTERNATIVE TREATMENT OF HEAT FLOW FOR CHARGE TRANSPORT IN SEMICONDUCTOR DEVICES (POSTPRINT)

5a. CONTRACT NUMBER

5b. GRANT NUMBER
FA8750-06-1-0085

5c. PROGRAM ELEMENT NUMBER
62500F

6. AUTHOR(S)
Matt Grupen

5d. PROJECT NUMBER
5028

5e. TASK NUMBER
RL

5f. WORK UNIT NUMBER
528DSN04

7. PERFORMING ORGANIZATION NAME(S) AND ADDRESS(ES)
Electro-optic Components Technology Branch (AFRL/RYDP)
Aerospace Components Division
Air Force Research Laboratory, Sensors Directorate
Wright-Patterson Air Force Base, OH 45433-7320
Air Force Materiel Command, United States Air Force

8. PERFORMING ORGANIZATION REPORT NUMBER

9. SPONSORING/MONITORING AGENCY NAME(S) AND ADDRESS(ES)
Air Force Research Laboratory
Sensors Directorate
Wright-Patterson Air Force Base, OH 45433-7320
Air Force Materiel Command
United States Air Force

Air Force Office of Scientific Research (AFOSR)

10. SPONSORING/MONITORING AGENCY ACRONYM(S)
AFRL/RYDP, AFOSR

11. SPONSORING/MONITORING AGENCY REPORT NUMBER(S)
AFRL-RY-WP-TP-2011-1007

12. DISTRIBUTION/AVAILABILITY STATEMENT
Approved for public release; distribution unlimited.

13. SUPPLEMENTARY NOTES
Journal article published in *Journal of Applied Physics* 106 (2009).

 This work is one of a number of manuscripts published in peer-reviewed journals as a result of in-house work on technical report AFRL-RY-WP-TR-2010-1195. This paper contains color and is available to the public.

14. ABSTRACT
A unique thermodynamic model of Fermi gases suitable for semiconductor device simulation is presented. Like other models, such as drift diffusion and hydrodynamics, it employs moments of the Boltzmann transport equation derived using the Fermi–Dirac distribution function. However, unlike other approaches, it replaces the concept of an electron thermal conductivity with the heat capacity of an ideal Fermi gas to determine heat flow. The model is used to simulate a field-effect transistor and show that the external current-voltage characteristics are strong functions of the state space available to the heated Fermi distribution.

15. SUBJECT TERMS

16. SECURITY CLASSIFICATION OF:			17. LIMITATION OF ABSTRACT:	18. NUMBER OF PAGES	19a. NAME OF RESPONSIBLE PERSON (Monitor)
a. REPORT	b. ABSTRACT	c. THIS PAGE			Nicholas G. Usechak
Unclassified	Unclassified	Unclassified	SAR	14	19b. TELEPHONE NUMBER *(Include Area Code)* N/A

Standard Form 298 (Rev. 8-98)
Prescribed by ANSI Std. Z39-18

An alternative treatment of heat flow for charge transport in semiconductor devices

Matt Grupen[a)]
Air Force Research Laboratory, 2241 Avionics Circle, Wright-Patterson AFB, Ohio 45433, USA

(Received 22 September 2009; accepted 6 November 2009; published online 18 December 2009)

A unique thermodynamic model of Fermi gases suitable for semiconductor device simulation is presented. Like other models, such as drift diffusion and hydrodynamics, it employs moments of the Boltzmann transport equation derived using the Fermi–Dirac distribution function. However, unlike other approaches, it replaces the concept of an electron thermal conductivity with the heat capacity of an ideal Fermi gas to determine heat flow. The model is used to simulate a field-effect transistor and show that the external current-voltage characteristics are strong functions of the state space available to the heated Fermi distribution. © *2009 American Institute of Physics*.
[doi:10.1063/1.3270404]

I. INTRODUCTION

Throughout most of its history, macroscopic simulation of semiconductor device physics has focused on solving the Boltzmann transport equation using the Fermi–Dirac distribution function or its Maxwell–Boltzmann approximation.[1,2] Representing mobile charge ensembles with these distribution functions is tantamount to treating them as ideal gases. A three-dimensional ideal Fermi gas is spherically symmetric in momentum space, and its distribution in energy is determined entirely by its chemical potential and temperature. Inserting the Fermi–Dirac distribution into the Boltzmann equation and solving for spatial variations in the chemical potential and temperature form the bases for drift-diffusion and hydrodynamic charge transport theories.[2,3] These theories offer accurate approximations when the rate that charges interact within a particular Fermi gas is much greater than the rate that charges are exchanged between gases. An ensemble of electrons localized in space and confined to an energy continuum can thermalize very rapidly if the density is high. While devices often contain high field regions where the density is low and the distribution can become non-Fermi-like, these generally occur between high density regions where the Fermi approximation is accurate. If the gas is permitted to heat and the second law of thermodynamics is enforced during the transition from one Fermi distribution to another, the use of Fermi gases throughout provides a reasonable approximation of the electron dynamics. Furthermore, when the electron state space includes forbidden energy gaps where no states exist, the Fermi gas approach is flexible enough to accommodate separate Fermi distributions for different bands of states separated in energy. This allows the transport model to treat bipolar devices for which distributions of electrons in the conduction band and holes in the valence band are represented by separate Fermi functions with different chemical potentials and temperatures. An analogous approach has also been used to accurately represent the capture of injected electrons into the active regions of quantum well laser diodes by assigning separate Fermi distributions to the bound states within the well and the continuum of propagating states above the well's energy barriers.[4] The flexibility, effectiveness, and relative computational efficiency of this Fermi–Dirac approach to charge transport are evidenced by its widespread use in macroscopic semiconductor device simulators, including computer aided design software applications such as PISCES,[5] DESSIS,[6] and their commercial descendants.

To solve for spatial variations in chemical potentials and temperatures, device simulators typically couple Poisson's equation for the electrostatic fields to conservation relations for mobile charge densities and energies. Unlike stochastic solutions of the Boltzmann equation,[7–10] solutions using the Fermi distribution are only physically self-consistent when they explicitly enforce certain necessary conditions of ideal gas thermodynamics. One condition is that heat flows between gases with different temperatures. In a seminal paper, Stratton[11] expressed this heat flow as $\kappa(T)\nabla T$, where κ is the thermal conductivity of electrons and T is the electron temperature. To determine κ, Stratton[11] made use of the Wiedemann–Franz–Lorentz law, an empirical observation that relates the thermal and electrical conductivities of a metal to its temperature. The great majority of Fermi gas treatments of energy transport have adopted this concept of an electron thermal conductivity, and a great deal of research on hydrodynamics has involved determining the proper mathematical representation of this conductivity and the moments of the Boltzmann equation required to complete the model.[2,12]

This paper proposes an alternative treatment of heat flow that replaces the concept of an electron thermal conductivity with the Fermi distribution's heat capacity. The electronic equations, including electron density and kinetic energy fluxes, will be presented. Then it will be shown that considering the definition of heat capacity for a Fermi gas and relating it to these fluxes suggests an expression for heat flow that completes the thermodynamic model. To demonstrate this approach, a GaAs metal-semiconductor field-effect transistor (MESFET) will be simulated. Different parabolic band

[a)]Electronic mail: matthew.grupen@wpafb.af.mil.

structures will be considered to show how the interaction of the Fermi gases with their state space can affect the external characteristics of the device.

II. DEVICE EQUATIONS AND CHARGE FLUXES

A semiconductor device can be simulated by solving equations for electrostatics as well as charge density and energy conservation. Electrostatics may be represented by Poisson's equation

$$\nabla \cdot \epsilon \boldsymbol{E} = q(p - n + N_D^+ - N_A^-), \tag{1}$$

where ϵ is the dielectric constant, $\boldsymbol{E}$ is the electric field, q is the electron charge, p is the density of mobile holes, n is the electron density, N_D^+ is the density of ionized donor impurities, and N_A^- is the ionized acceptor concentration. The carrier densities may be computed by assuming Fermi–Dirac distributions, constant effective mass, and parabolic band structures. For electrons,

$$n = \frac{\sqrt{2}m_n^{3/2}}{\pi^2\hbar^3}\int_{E_C}^{\infty}\frac{\sqrt{E-E_C}}{\exp\left(\frac{E-F}{k_BT}\right)+1}dE = N_C(k_BT)^{3/2}\mathcal{F}_{1/2}(\eta), \tag{2}$$

where m_n is the effective mass, $\hbar$ is Planck's constant, E is the electron energy, E_C is the conduction band edge, F is the chemical potential (Fermi level), k_B is the Boltzmann constant, T is the electron temperature, and N_C is the effective density of states. The Fermi integral of order j is defined as

$$\mathcal{F}_j(\eta) = \int_0^{\infty}\frac{\epsilon^j}{e^{\epsilon-\eta}+1}d\epsilon, \tag{3}$$

evaluated for the unitless parameter $\eta \equiv (F-E_C)/(k_BT)$. The electron internal energy density is

$$E_n = \frac{\sqrt{2}m_n^{3/2}}{\pi^2\hbar^3}\int_{E_C}^{\infty}\frac{(E-E_C)^{3/2}}{\exp\left(\frac{E-F}{k_BT}\right)+1}dE = N_C(k_BT)^{5/2}\mathcal{F}_{3/2}(\eta). \tag{4}$$

Electron continuity and energy conservation are given by

$$-\frac{\partial n}{\partial t} = \nabla \cdot \boldsymbol{J}_n + U, \tag{5}$$

$$-\frac{\partial E_n}{\partial t} = q\boldsymbol{E}\cdot\boldsymbol{J}_n + \nabla\cdot\boldsymbol{S}_n^{\mathrm{tot}} + \langle E_n\rangle U + \frac{E_n(T)-E_n(T_{\mathrm{lat}})}{\tau_E}, \tag{6}$$

where $\boldsymbol{J}_n$ is the electron flux density, U is the net electron-hole recombination rate, $\boldsymbol{S}_n^{\mathrm{tot}}$ is the total electron energy flux, $\langle E_n\rangle$ is the average kinetic energy per electron, T_{lat} is the lattice temperature, and τ_E is the average lifetime for electron energy loss from phonon emission. Here Eqs. (5) and (6) have been simply stated as conservation relations, but they can be derived from the zeroth and second moments, respectively, of the Boltzmann equation.[13] Similar expressions exist for mobile holes.

Mobile charge fluxes can be obtained from the first moment of the Boltzmann equation using the momentum relaxation time and effective mass approximations.[13] Neglecting any magnetic field and the associated Lorentz force, the first moment for electrons in steady state can be expressed as

$$\boldsymbol{J}_n = \frac{1}{4\pi^3}\int_{\boldsymbol{k}}\boldsymbol{v}\left[\frac{q\tau_k}{\hbar}\boldsymbol{E}\cdot\nabla_{\boldsymbol{k}}f - \tau_k\boldsymbol{v}\cdot\nabla f\right]d\boldsymbol{k}, \tag{7}$$

where the integral is over all momentum vectors $\boldsymbol{k}$, $\boldsymbol{v}$ is electron velocity, τ_k is the momentum relaxation time, and $\nabla_{\boldsymbol{k}}f$ denotes the gradient in momentum space of the Fermi distribution function f. Although τ_k is generally a function of $\boldsymbol{k}$, for simplicity it will be considered a constant. Also, a simple constant effective mass band structure is assumed such that kinetic energy $E = m_n|\boldsymbol{v}|^2/2$ and momentum $\hbar\boldsymbol{k} = m_n\boldsymbol{v}$. The integral over $\boldsymbol{k}$ can then be transformed into an integral over E, and the flux can be expressed as

$$\boldsymbol{J}_n = -\frac{q\tau_k}{m_n}N_C\left[\boldsymbol{E}(k_BT)^{3/2}\mathcal{F}_{1/2}(\eta) + \nabla\frac{2}{3}\frac{(k_BT)^{5/2}}{q}\mathcal{F}_{3/2}(\eta)\right]. \tag{8}$$

For numerical solution, this differential equation is represented in discrete form on the edges of a mesh that appropriately represents the device. An adaptation of the Scharfetter–Gummel method[14,15] can be used to express Eq. (8) in discrete form. To this end, Eq. (8) is recast as a differential equation for electron density (2) as follows:

$$\boldsymbol{J}_n = -\frac{q\tau_k}{m_n}\left\{\left[\boldsymbol{E} + \nabla\left(\frac{2}{3}\frac{\mathcal{F}_{3/2}}{\mathcal{F}_{1/2}}\frac{k_BT}{q}\right)\right]n + \left(\frac{2}{3}\frac{\mathcal{F}_{3/2}}{\mathcal{F}_{1/2}}\frac{k_BT}{q}\right)\nabla n\right\}. \tag{9}$$

If the flux is assumed to be constant along a given edge that connects mesh points 1 and 2, then Eq. (9) can be solved for the electron density along the edge and the corresponding electron flux. The resulting discrete form of the net flux from point 1 to point 2 can be written as

$$J_n^{1\to 2} = \frac{q\tau_k}{m_n}\left(\frac{2}{3}\frac{\mathcal{F}_{3/2}}{\mathcal{F}_{1/2}}\frac{k_BT}{q}\right)_{\mathrm{av}}\frac{1}{L}[B(\xi_n)n_1 - B(-\xi_n)n_2] = J_1(F_1,T_1,F_2,T_2) - J_2(F_1,T_1,F_2,T_2), \tag{10}$$

where L is the length of the edge, the notation $(x)_{\mathrm{av}}$ denotes the average[16] of quantity x evaluated at points 1 and 2, and $B(\xi) = \xi/[\exp(\xi)-1]$ is the Bernoulli function. For electrons, the argument of the Bernoulli function is given by

$$\xi_n = L\left(\frac{3}{2}\frac{\mathcal{F}_{1/2}}{\mathcal{F}_{3/2}}\frac{q}{k_BT}\right)_{\mathrm{av}}\left[E_{1\to 2} + \frac{1}{L}\Delta\left(\frac{2}{3}\frac{\mathcal{F}_{3/2}}{\mathcal{F}_{1/2}}\frac{k_BT}{q}\right)\right], \tag{11}$$

where $E_{1\to 2}$ is the electric field directed from point 1 to point 2, and the notation $\Delta(x) = x_2 - x_1$ denotes the difference between the values of x evaluated at the two points. Note that net flux (10) appears as the difference between electrons emitted from one distribution J_1 and those emitted from the other J_2. Each component is a function of the chemical potentials and temperatures from both distributions because of the average prefactor and the arguments of the Bernoulli functions. An analogous charge flux exists for mobile holes.

For a Fermi gas at constant volume,[17] the ideal gas law specifies the total energy flux density $\boldsymbol{S}_n^{\text{tot}}$ as the sum of the internal (kinetic) energy flux density $\boldsymbol{S}_{\text{kin}}$ and the heat flow density $\boldsymbol{S}_{\text{heat}}$. The internal energy flux can be obtained from the third moment of the Boltzmann equation. To derive this moment, the procedure outlined above is repeated, but the Boltzmann equation is multiplied by both electron velocity $\boldsymbol{v}$ and kinetic energy E as follows:

$$\boldsymbol{S}_{\text{kin}} = \frac{1}{4\pi^3}\int_{\boldsymbol{k}} E\boldsymbol{v}\left[\frac{q\tau_k}{\hbar}\boldsymbol{E}\cdot\nabla_{\boldsymbol{k}}f - \tau_k\boldsymbol{v}\cdot\nabla f\right]d\boldsymbol{k} = -\frac{q\tau_k}{m_n}\left\{\left[\frac{5}{3}\boldsymbol{E} + \nabla\left(\frac{2}{3}\frac{\mathcal{F}_{5/2}}{\mathcal{F}_{3/2}}\frac{k_BT}{q}\right)\right]E_n + \left(\frac{2}{3}\frac{\mathcal{F}_{5/2}}{\mathcal{F}_{3/2}}\frac{k_BT}{q}\right)\nabla E_n\right\}. \tag{12}$$

Applying the Scharfetter–Gummel method, this flux is assumed constant along a mesh edge, reducing Eq. (12) to a differential equation for E_n whose boundary conditions are the energy densities at the edge's end points. Solving this differential equation for the flux gives

$$S_{\text{kin}}^{1\to2} = \frac{q\tau_k}{m_n}\left(\frac{2}{3}\frac{\mathcal{F}_{5/2}}{\mathcal{F}_{3/2}}\frac{k_BT}{q}\right)_{\text{av}}\frac{1}{L}[B(\xi_E)E_{n,1} - B(-\xi_E)E_{n,2})] = S_1(F_1,T_1,F_2,T_2) - S_2(F_1,T_1,F_2,T_2), \tag{13}$$

where $E_{n,1}$ and $E_{n,2}$ are the energy densities at points 1 and 2, respectively, and the argument of the Bernoulli function is given by

$$\xi_E = L\left(\frac{3}{2}\frac{\mathcal{F}_{3/2}}{\mathcal{F}_{5/2}}\frac{q}{k_BT}\right)_{\text{av}}\left[\frac{5}{3}E_{1\to2} + \frac{1}{L}\Delta\left(\frac{2}{3}\frac{\mathcal{F}_{5/2}}{\mathcal{F}_{3/2}}\frac{k_BT}{q}\right)\right]. \tag{14}$$

Analogous to electron flux, the net internal energy flux has the form of internal energy emitted from distribution 1 minus that emitted from distribution 2, and cross coupling occurs through the prefactor and Bernoulli terms. A similar internal energy flux can be derived for mobile holes.

III. HEAT FLOW DENSITY

The remaining energy flux required to complete the electron thermodynamics is the heat flow. Instead of invoking the concept of an electron thermal conductivity to compute the heat flow, this paper proposes an alternative view. In hydrodynamics, charges moving through real space are removed from one Fermi gas with a particular temperature and transferred to another with a different temperature. When electrons move from a Fermi distribution at point 1 to another at point 2, they must be heated or cooled from their initial to their final temperature. If $T_1 < T_2$, electrons at point 2 must provide energy to the injected electrons, and this constitutes a flow of heat from Fermi gas 2 to Fermi gas 1. If $T_2 < T_1$, the converse is true. Note that the heat flow opposes the temperature gradient regardless of the direction of electron flux.

The heat capacity C_{el} of a Fermi distribution[18] determines the energy E_{heat} required to heat it from one temperature to another,

$$E_{\text{heat}} = \int_{T_i}^{T_f} C_{\text{el}}dT = \int_{T_i}^{T_f}\left[\frac{1}{4\pi^3}\int_{\boldsymbol{k}}(E-F)\frac{df}{dT}d\boldsymbol{k}\right]dT = [E_n(T) - Fn(T)]_{T_i}^{T_f}, \tag{15}$$

where $T_{i(f)}$ is the initial (final) temperature. Similarly, as pointed out in Seeger's discussion of energy transport in electron gases,[19] heat flow density is the difference between the internal and free energy flux densities. With these ideas in mind, this paper proposes that heat flow can be obtained from Eqs. (10) and (13) simply by evaluating their different components at their respective initial and final temperatures

$$\begin{aligned} S_{\text{heat}}^{1\to2} = &-\int_{T_1}^{T_2}\frac{d}{dT}[S_1(F_1,T,F_2,T_2) - (F_1 - E_{C,1})J_1(F_1,T,F_2,T_2)]dT \\ &+\int_{T_2}^{T_1}\frac{d}{dT}[S_2(F_1,T_1,F_2,T) - (F_2 - E_{C,2})J_2(F_1,T_1,F_2,T)]dT = S_1(F_1,T_1,F_2,T_2) \\ &- S_1(F_1,T_2,F_2,T_2) - (F_1 - E_{C,1})[J_1(F_1,T_1,F_2,T_2) - J_1(F_1,T_2,F_2,T_2)] + S_2(F_1,T_1,F_2,T_1) \\ &- S_2(F_1,T_1,F_2,T_2) - (F_2 - E_{C,2})[J_2(F_1,T_1,F_2,T_1) - J_2(F_1,T_1,F_2,T_2)]. \end{aligned} \tag{16}$$

By expressing heat flow as the difference between internal energy and free energy fluxes evaluated at different temperature limits, including its effects becomes highly formulaic. For any transport mechanism that can be represented as integrals over the energy spectra of two Fermi distributions exchanging charges, the associated heat flow can be readily determined from Eq. (16). For example, at abrupt heterojunctions or Schottky barriers, an ill-defined electric field makes drift-diffusion theory inappropriate, and charge flux can be better represented by thermionic emission. At the conduction band discontinuity, the net electron flux from the low L to the high H side of the interface may be represented as

$$\begin{aligned} J_{\text{te}} = J_{L\to H} - J_{H\to L} = &\frac{1}{2\pi^2}\frac{m_n}{\hbar^3}\left[(k_BT_L)^2\mathcal{F}_1\left(\frac{F_L - E_{C,H}}{k_BT_L}\right) - (k_BT_H)^2\mathcal{F}_1\left(\frac{F_H - E_{C,H}}{k_BT_H}\right)\right] = J_L(F_L,T_L) \\ &- J_H(F_H,T_H). \end{aligned} \tag{17}$$

Note that the unitless arguments of both Fermi integrals are evaluated with respect to the conduction band edge on the high side of the interface $E_{C,H}$. The corresponding internal energy flux is given by

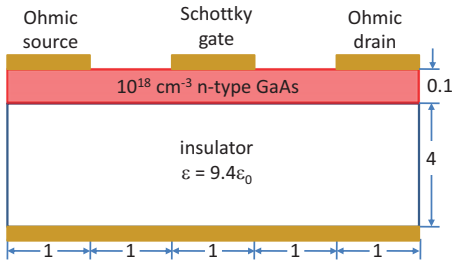

FIG. 1. (Color online) Approximation of a GaAs MESFET. Dimensions are in microns. The Schottky barrier height is assumed to be 1 eV, and each contact is treated as a perfect electrical conductor.

$$S_{\text{te,kin}} = S_{L\to H} - S_{H\to L} = \frac{1}{2\pi^2}\frac{m_n}{\hbar^3}\left[(k_B T_L)^3 \mathcal{F}_2\left(\frac{F_L - E_{C,H}}{k_B T_L}\right) - (k_B T_H)^3 \mathcal{F}_2\left(\frac{F_H - E_{C,H}}{k_B T_H}\right)\right] = S_L(F_L, T_L) - S_H(F_H, T_H). \tag{18}$$

Following the procedure indicated in Eq. (16), the thermionic emission heat flow can be expressed as

$$\begin{aligned} S_{\text{te,heat}} &= S_L(F_L,T_L) - S_L(F_L,T_H) - (F_L - E_{C,H})[J_L(F_L,T_L) - J_L(F_L,T_H)] + S_H(F_H,T_L) - S_H(F_H,T_H) - (F_H - E_{C,H})[J_H(F_H,T_L) - J_H(F_H,T_H)] \\ &= \frac{1}{2\pi^2}\frac{m_n}{\hbar^3}\Bigg\{(k_B T_L)^3 \mathcal{F}_2\left(\frac{F_L - E_{C,H}}{k_B T_L}\right) - (k_B T_H)^3 \mathcal{F}_2\left(\frac{F_L - E_{C,H}}{k_B T_H}\right) - (F_L - E_{C,H}) \times \left[(k_B T_L)^2 \mathcal{F}_1\left(\frac{F_L - E_{C,H}}{k_B T_L}\right) - (k_B T_H)^2 \mathcal{F}_1\left(\frac{F_L - E_{C,H}}{k_B T_H}\right)\right] \\ &\quad + (k_B T_L)^3 \mathcal{F}_2\left(\frac{F_H - E_{C,H}}{k_B T_L}\right) - (k_B T_H)^3 \mathcal{F}_2\left(\frac{F_H - E_{C,H}}{k_B T_H}\right) - (F_H - E_{C,H}) \times \left[(k_B T_L)^2 \mathcal{F}_1\left(\frac{F_H - E_{C,H}}{k_B T_L}\right) - (k_B T_H)^2 \mathcal{F}_1\left(\frac{F_H - E_{C,H}}{k_B T_H}\right)\right]\Bigg\}, \end{aligned} \tag{19}$$

where the chemical potential of each distribution is measured from the point of zero kinetic energy, which for thermionic emission is always $E_{C,H}$. The distribution on the low side feels the effects of the barrier height through a potential energy term $(E_{C,H}-E_{C,L})J_{\text{te}}$, which plays the same role in its energy balance equation as $q\boldsymbol{E}\cdot\boldsymbol{J}_n$ plays in Eq. (6).

IV. RESULTS AND DISCUSSION

To test the energy transport model, the simple GaAs MESFET structure shown schematically in Fig. 1 was simulated by solving Eqs. (1), (5), and (6) self-consistently using the full-Newton method. Mobile holes in the valence band and lattice heating were not considered. Fluxes defined by Eqs. (17)–(19) were applied at the Schottky gate interface while fluxes (10), (13), and (16) were used in the GaAs bulk. A Schottky barrier height of 1 eV was used for the gate, and all contacts were treated as perfect electrical conductors with electron temperatures equal to 300 K. As represented in Fig. 2, conduction band electrons occupied simple parabolic valleys extending to infinite energy. Different simulations included different valleys. The momentum relaxation time τ_k was treated as a constant, and its value was determined by assuming a value of 8500 $\text{cm}^2/(\text{V s})$ for the Γ valley's low field electron mobility $\mu_n = q\tau_k/m_n$ and assuming an effective mass of $m_n = 0.067m_0$, where m_0 is the free electron mass. These simulations exhibited stable quadratic convergence for all applied bias conditions.

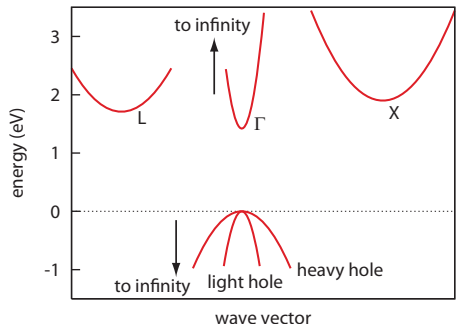

FIG. 2. (Color online) Simple effective mass band structure to represent GaAs. Each band extends to infinite carrier energy. An effective mass of $0.067m_0$ is used for the Γ valley and $0.85m_0$ is used for the L and X valleys. The L and X valley minima are 0.29 and 0.48 eV, respectively, above the Γ valley minimum.

For the initial set of simulations, only the Γ valley was considered. The drain current versus drain voltage for different gate biases is shown in Fig. 3. Two striking features of these curves are the superlinear behavior at low drain voltages and the low differential resistance at higher drain voltages, i.e., weak current saturation beyond pinch-off. Both of these features can be associated with the constant momentum relaxation time τ_k and the simplified band structure. At low drain voltage, before the channel is pinched off, increasing drain voltage causes electrons to heat up, increasing their

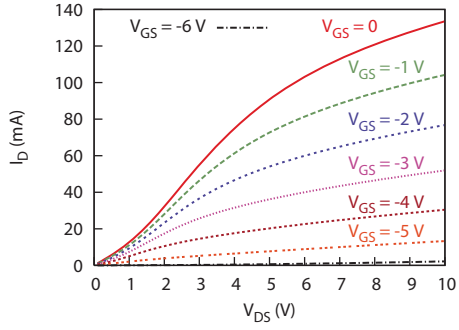

FIG. 3. (Color online) MESFET drain current as a function of drain voltage for different gate biases. In this simulation, the X and L valleys were ignored and only an infinite parabolic Γ valley was available to conduction band electrons.

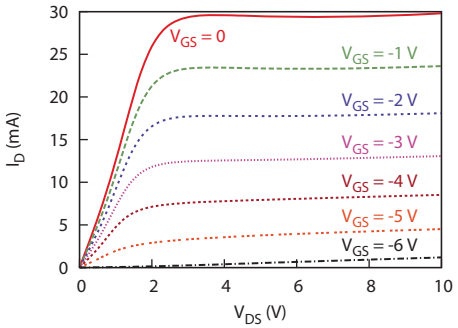

FIG. 4. (Color online) MESFET drain current as a function of drain voltage for different gate biases. In these simulations, the X and L valleys were considered as well as the Γ valley in the GaAs conduction band.

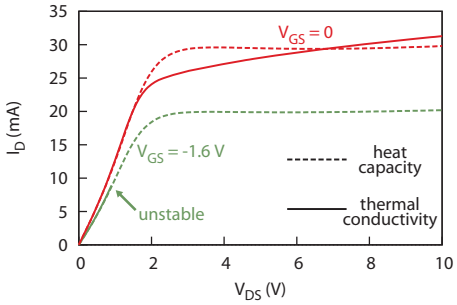

FIG. 6. (Color online) MESFET drain current as a function of drain voltage for different gate biases computed with both the electron heat capacity model (dashed) and the electron thermal conductivity model (solid) for heat flow. These simulations used the infinite Γ, X, and L valley model for the GaAs conduction band structure. The label "unstable" indicates the point at which the thermal conductivity model diverged and produced no further solutions.

average velocity. Since τ_k is constant, Eq. (7) shows that an increasing average velocity combined with the increasing electric field produces a superlinear drain current. At higher drain voltages, the electron density in the pinch-off region is reduced, but the high fields there can heat the electrons to well over 1000 K. Because of the constant τ_k and the simplified band structure, there are unlimited high mobility states available to the hot carriers, preventing the drain current from saturating. In reality, τ_k should decrease with increasing electron energy and suppress both superlinear behavior at low drain voltages and the channel conductance at higher voltages.

A second set of simulations included the X and L valleys along with the Γ valley in Fig. 2. Although the same constant momentum relaxation time τ_k was used, an increased effective mass $m_n=0.85m_0$ was assigned to the X and L valleys, causing their densities of states to be higher and their mobilities to be lower than the Γ valley. The resulting drain current characteristics are shown in Fig. 4. There is still some indication of superlinearity at low drain voltages because most electrons are in the Γ valley in this bias range, and as described above, the constant τ_k along with increasing average velocity from electron heating combines to produce this effect. However, these simulations show increased differential resistance at higher drain voltages, and the drain currents saturate at much lower values. The saturation can be explained by Fig. 5, which shows electron density spectra at a point corresponding to the pinch-off region of the channel. The spectra were computed for different drain voltages and

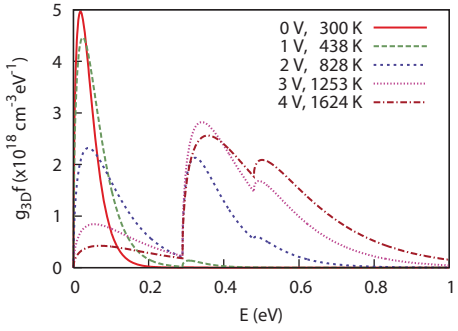

FIG. 5. (Color online) Product of the distribution function and the density of states as a function of electron energy at a point in the pinch-off region of the channel for zero gate bias and different drain voltages computed with the three parabolic valley conduction band model.

their labels include the corresponding electron temperatures. It bears mentioning that each point in the simulation has only one electron chemical potential and temperature, meaning the Γ, X, and L valleys share the same distribution function. The different valleys only determine the states available to the distribution function. As drain voltage increases, heating causes an increasing fraction of the total electron population to occupy the low mobility X and L valleys. Although the distribution function is always larger in the lower energy Γ valley, the larger density of states in the X and L valleys causes them to contain the majority of electrons at sufficiently high temperatures. Consequently, as increasing electric field in the channel increases electron temperature, more carriers occupy the high energy X and L valleys, the average electron mobility decreases, and the drain current saturates.

By way of comparison, the simulations that produced Fig. 4 were repeated using the phenomenological treatment of heat flow $\boldsymbol{S}_{\text{heat}}=-\kappa\nabla T$ with an electron thermal conductivity given by

$$\kappa = q\mu_n n\left(\frac{k_B}{q}\right)^2\left(\frac{5}{2}+\nu\right)T. \tag{20}$$

The parameter ν is customarily chosen to best account for the effect of the electron scattering rate's energy dependence on the Lorenz number.[11,20,21] Following a similar simulation by Jyegal and DeMassa,[21] ν was set equal to zero. Note that this form for heat flow can be applied only to drift diffusion in the bulk regions of the device. For thermionic emission at the Schottky interface, the temperature is discontinuous and its gradient ill defined. As a result, electrons on the Schottky gate boundary were held at room temperature for the electron thermal conductivity simulations. Computed drain currents for different drain and gate voltages are shown in Fig. 6. Some key features are the more gradual onset of saturation, the reduced differential resistance after pinch-off, and the numerical instability exhibited by the electron thermal conductivity model. For increasingly negative gate biases, the electron thermal conductivity model became unstable at lower drain voltages.

The drain currents in Fig. 6 can be understood in terms of the relationship between electron temperature and average velocity that was previously used to discuss Figs. 3 and 4.

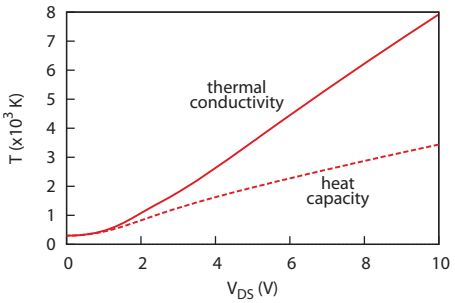

FIG. 7. (Color online) The electron temperature at a point in the MESFET pinch-off region calculated for zero gate bias and different drain voltages using the infinite Γ, *X*, and *L* valley model for band structure and using both the electron thermal conductivity model (solid) and the electron heat capacity model (dashed) for heat flow.

Figure 7 shows electron temperatures at a mesh point in the pinch-off region computed for zero gate bias and different drain voltages using both the electron thermal conductivity and heat capacity models. The thermal conductivity model produces significantly more electron heating. At lower drain voltages, this causes the lower mobility *X* and *L* valleys to become populated sooner and causes a reduction in the drain current near the onset of pinch-off when compared to the heat capacity model. As indicated by Fig. 5, at higher drain voltages, the electrons in the pinch-off region occupy mostly the *X* and *L* valleys. Therefore, the currents at higher drain biases are dominated by the average velocities in these valleys. Since the thermal conductivity model continues to heat the electrons at an accelerated rate and since the band structure model allows the *X* and *L* valleys to extend to infinite energy, the distribution function can access higher velocity states and the drain current continues to increase even in saturation.

The differences between electron temperatures produced by the electron thermal conductivity and the electron heat capacity models are not altogether surprising when the origins of the thermal conductivity concept are considered. A thermal conductivity of the form expressed in Eq. (20) was motivated by the empirical observation relating thermal and electrical conductivities in metals. A metal contains a degenerate Fermi gas of conducting electrons. From its definition in terms of its internal and free energies (15), the heat capacity of a degenerate Fermi gas is relatively low. However, the MESFET contains depletion regions under the gate and in the pinched off channel where the electron densities are many orders of magnitude less than in a metal, and the heat capacities per electron of the rarefied gases in these regions are much higher. Since the thermal conductivity model (20) contains no information about the electron heat capacity, the low electron density in the depleted regions requires a larger temperature gradient to provide a given amount of heat flow. The alternative model, on the other hand, does include the enhanced heat capacity of the rarefied electron gas and requires a smaller temperature gradient to achieve the same heat flow. Moreover, it might also be argued that a model based on Fermi gas thermodynamics must consider its heat capacity in order to achieve self-consistency and maintain numerical stability.

V. CONCLUSION

Unlike stochastic solutions of electron transport, solutions based on Fermi distributions require certain thermodynamic conditions to be explicitly enforced. One is that heat flow between Fermi gases must be included in the total energy flux in order to fulfill the second law of thermodynamics. For semiconductor device simulation, computing this heat flow has generally involved defining an electron thermal conductivity and multiplying it by a gradient in electron temperature. Determining the precise nature of the thermal conductivity has often involved introducing additional degrees of freedom to the model in the form of higher order moments of the Boltzmann equation. This paper proposed a different interpretation of heat flow between Fermi gases.

Instead of invoking an electron thermal conductivity, the heat capacity of the Fermi distribution was considered. This can be precisely defined in terms of the difference between its internal and its free energies. When two Fermi gases exchange charges, the rates that heat must be provided to heat and cool those charges can then be determined by simply comparing their kinetic and free energy flux densities evaluated at their initial and final temperatures. For energy transport based on the drift and diffusion of Fermi distributions, i.e., the hydrodynamic model, this interpretation of heat flow means moments 0–3 of the Boltzmann equation are sufficient to describe the charge thermodynamics.

In addition to drift-diffusion transport, the same basic scheme can be used to determine the heat flow associated with any transport mechanism that can be expressed as integrals over the energy spectra of two Fermi gases. This was shown for the case of thermionic emission at an abrupt heterojunction. Although not implemented in this paper, the method could also be applied to scattering between different valleys in the semiconductor band structure. If different electron chemical potentials and temperatures were assigned to the different valleys, scattering between the valleys could be explicitly considered by integrating the scattering rate over the densities and occupation probabilities of the initial and final states. Although this is transport in momentum space instead of real space, it still involves integrating two interacting Fermi distributions over their energy spectra. As a result, the same comparisons of internal and free energy fluxes at the initial and final temperatures could be used to evaluate the heat exchange associated with the scattering process.

To demonstrate the model, a GaAs MESFET structure was simulated with simple parabolic valleys representing electron states in the conduction band. Each valley was assumed to have the same constant momentum relaxation time. All the simulations that used the electron heat capacity model for heat flow exhibited stable quadratic convergence of the coupled device equations. They also showed that the terminal currents depend significantly on the states available to the heated Fermi gases. This suggests that accurate band structures and energy dependent momentum relaxation rates could be key factors determining the accuracy of simulations based on Fermi distribution thermodynamics. Incorporating

more realistic dispersion relations will be the subject of continued research into this ideal Fermi gas formalism.

ACKNOWLEDGMENTS

This work was supported by the AFOSR Grant No. LRIR 09RY04COR.

[1]H. Gummel, IEEE Trans. Electron Devices **11**, 455 (1964).
[2]T. Grasser, T. W. Tang, H. Kosina, and S. Selberherr, Proc. IEEE **91**, 251 (2003).
[3]Y. P. Zhao, J. R. Watling, S. Kaya, A. Asenov, and J. R. Barker, Mater. Sci. Eng., B **72**, 180 (2000).
[4]M. Grupen and K. Hess, IEEE J. Quantum Electron. **34**, 120 (1998).
[5]M. R. Pinto, C. S. Rafferty, and R. W. Dutton, Stanford Electronics Laboratory Technical Report, 1984.
[6]S. Muller, K. Kells, A. Benvenuti, J. Litsios, U. Krumbein, A. Schenk, and W. Fichtner, DESSIS User's Manual, ISE TCAD Release 10.0 (2004).
[7]S. M. Goodnick, M. Saraniti, D. Vasileska, and S. Aboud, IEEE Potentials **22**, 12 (2009).
[8]J. D. Albrecht, P. P. Ruden, and K. F. Brennan, MRS Internet J. Nitride Semicond. Res. **4S1**, G6.6 (1999).
[9]K. Hess, *Monte Carlo Device Simulation: Full Band and Beyond* (Kluwer Academic, Norwell, MA, 1991).
[10]L. Bellomonte and R. M. Sperandeo-Mineo, Eur. J. Phys. **18**, 321 (1997).
[11]R. Stratton, Phys. Rev. **126**, 2002 (1962).
[12]M. Vasicek, J. Cervenka, M. Wagner, M. Karner, and T. Grasser, Solid-State Electron. **52**, 1606 (2008).
[13]K. Hess, *Advanced Theory of Semiconductor Devices* (Prentice-Hall, Englewood Cliffs, NJ, 1988).
[14]D. L. Scharfetter and H. K. Gummel, IEEE Trans. Electron Devices **16**, 64 (1969).
[15]S. Selberherr, *Analysis and Simulation of Semiconductor Devices* (Springer-Verlag, New York, 1984).
[16]The average is used because quantities x are assumed to vary linearly along a mesh edge, and the box integration method, used to represent carrier and energy conservation, requires fluxes to be evaluated at edge midpoints.
[17]The Fermi gas pressure is assumed to have a negligible effect on the volume of the semiconductor crystal, and therefore the role of mechanical work is not considered.
[18]C. Kittel and H. Kroemer, *Thermal Physics*, 2nd ed. (W.H. Freeman and Company, New York, 1980).
[19]K. Seeger, *Semiconductor Physics, An Introduction*, 3rd ed. (Springer-Verlag, New York, 1985).
[20]H. Z. Fardi, D. W. Winston, R. E. Hayes, and M. C. Hanna, IEEE Trans. Electron Devices **47**, 915 (2000).
[21]J. Jyegal and T. A. DeMassa, J. Appl. Phys. **76**, 4413 (1994).